INFALLING ENVELOPES AND PRE-MAIN SEQUENCE DISKS

NASA Grant NAGW-2306

Annual Report No. 5

For the period 1 September 1996 through 31 August 1997

and

Final Report

For the period 1 November 1990 through 30 September 1997

Principal Investigator

Lee W. Hartmann

October 1997

Prepared for

National Aeronautics and Space Administration

Washington, D.C. 20546

Smithsonian Institution
Astrophysical Observatory
Cambridge, Massachusetts 02138

The NASA Technical Officer for this Grant is Dr. Patricia Rogers, Code SLC, Headquarters, National Aeronautics and Space Administration, Washington, D.C. 20546

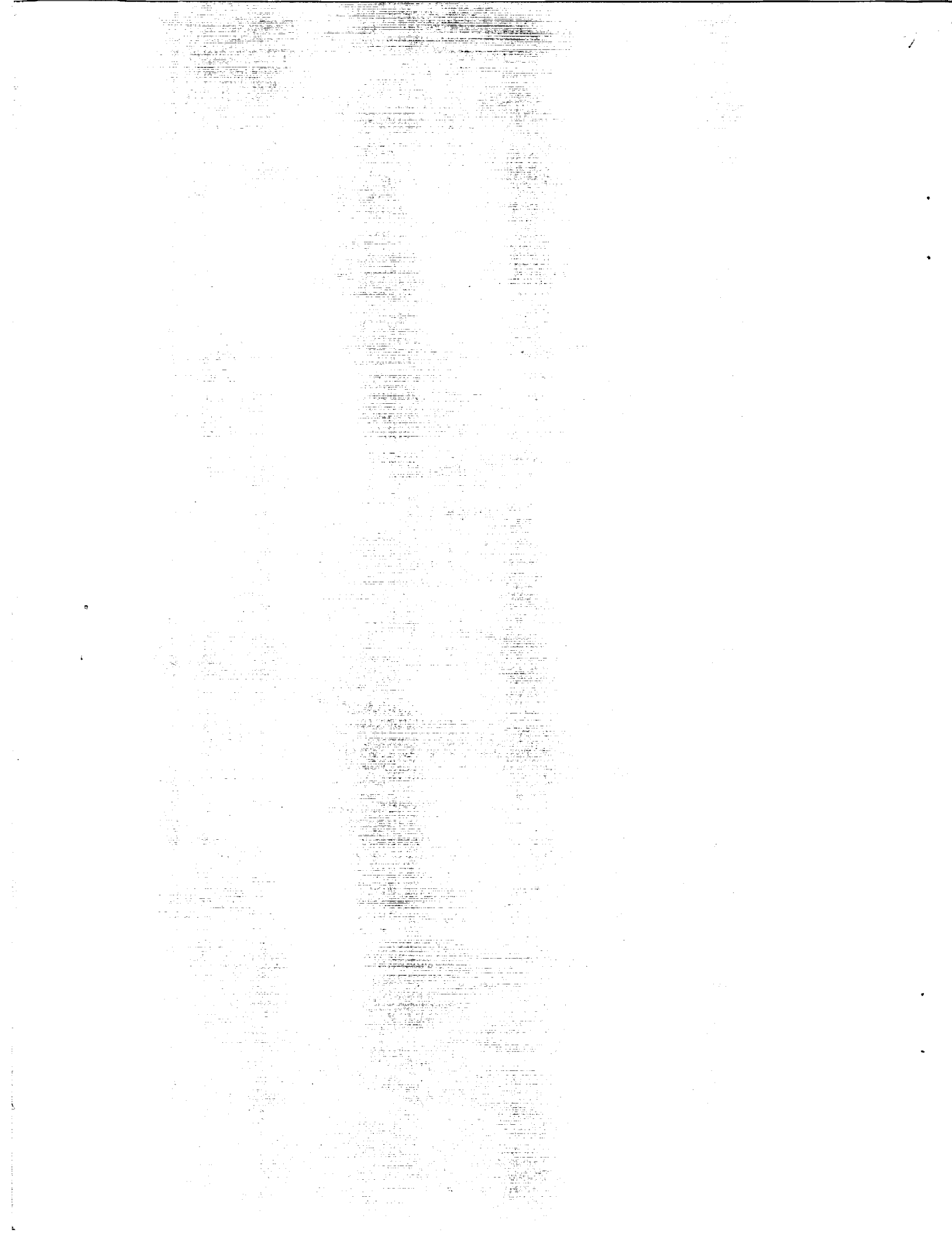

INFALLING ENVELOPES AND PRE-MAIN SEQUENCE DISKS

Annual Report 9/1/96 - 8/31/97, NAGW-2306, Hartmann et al.

The goal of this project is to understand the observed infrared emission of young stellar objects, and explore the implications of this emission for the evolution of dusty envelopes and circumstellar disks. We are using sophisticated radiative transfer methods to compare models with observations, thereby making critical tests of the standard picture of low-mass star formation.

DISK ACCRETION AND THE STELLAR BIRTHLINE

In Hartmann, Cassen, & Kenyon (1997), we presented a simplified analysis of some effects of disk accretion on the early evolution of fully-convective, low-mass pre-main sequence stars. Our analysis builds on the previous seminal work of Stahler (1988) but differs in that the accretion of material occurs over a small area of the stellar surface, such as through a disk or magnetospheric accretion column, so that most of the stellar photosphere is free to radiate to space. This boundary condition is similar to the limiting case considered by Palla & Stahler (1992) for intermediate-mass stars.

We argued that for a wide variety of disk mass accretion rates, material will be added to the star with relatively small amounts of thermal energy. Protostellar evolution calculated assuming this "low-temperature" limit of accretion generally follows the results of Stahler because of the thermostatic nature of deuterium fusion, which prevents protostars from contracting below a "birthline" in the HR diagram. Our calculated protostellar radii tend to fall below Stahler's at higher masses; the additional energy loss from the stellar photosphere in the case of disk accretion tends to make the protostar contract. The low-temperature disk accretion evolutionary tracks never fall below the deuterium-fusion birthline until the internal deuterium is depleted, but protostellar tracks can lie above the birthline in the HR diagram if the initial radius of the protostellar core is large enough, or if rapid disk accretion (such as might occur during FU Ori outbursts) adds significant amounts of thermal energy to the star. These possibilities cannot be ruled out by either theoretical arguments or observational constraints at present, so that individual protostars might evolve along a multiplicity of birthlines with a modest range of luminosity at a given mass.

Our results indicate that there are large uncertainties in assigning ages for the youngest stars from HR diagram positions, given the uncertainty in birthline positions. Our calculations also suggest that the relatively low disk accretion rates characteristic of T Tauri stars below the birthline cause low-mass stars to contract only slightly faster than normal Hayashi track evolution (Figure 5), so that ages for older pre-main sequence stars estimated from HR diagram positions are relatively secure.

NEAR-INFRARED EMISSION OF PROTOSTARS

In Calvet, Hartmann, & Strom (1997), we presented models for the thermal emission from dusty infalling envelopes around protostars, which indicate that the envelope emission can greatly exceed the stellar + disk photospheric emission at wavelengths $\sim 2\mu$m. We argued that this

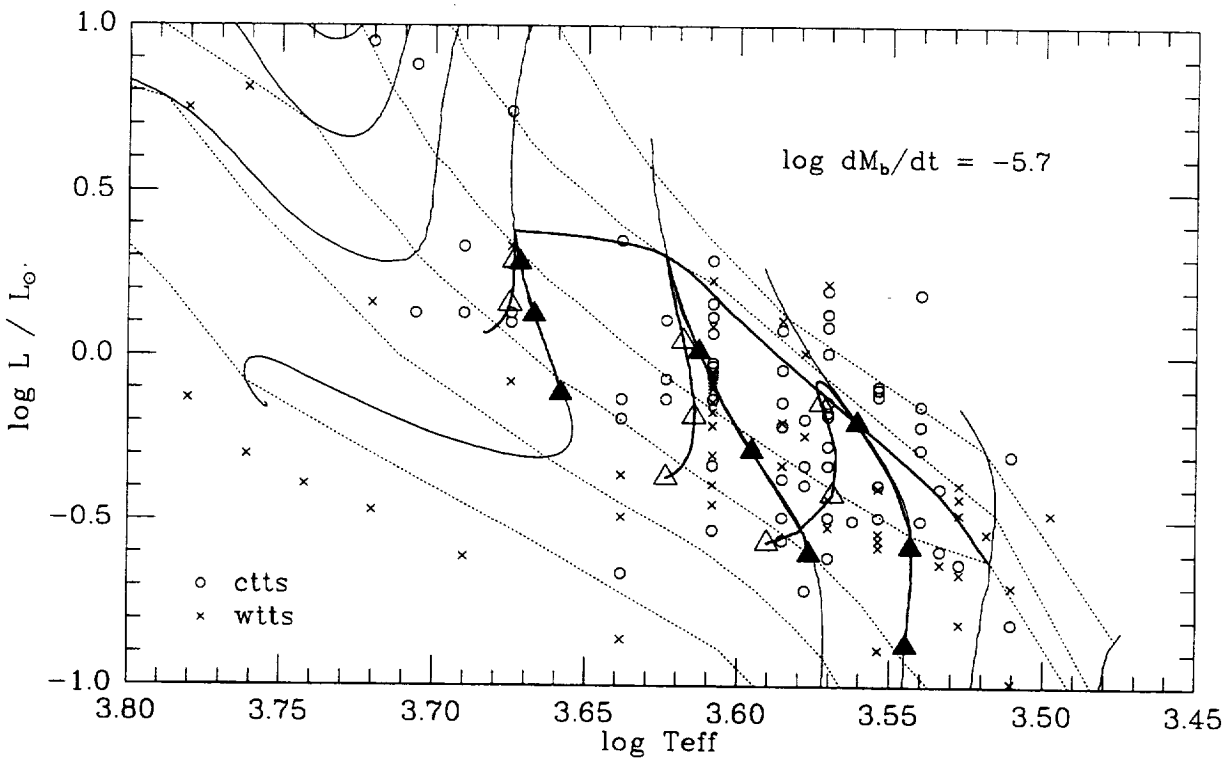

Figure 1: Stellar evolutionary tracks for low-temperature ($\alpha = 0$) disk accretion, compared with observations of T Tauri stars in the Taurus-Auriga star forming region. The evolutionary tracks are calculated interpolating in the CMA results to provide the calibration of $L_{phot}(M, R)$, producing small departures from the power-law calibration results shown in previous figures. The light solid lines show the pre-main sequence evolutionary tracks of D'Antona & Mazzitelli for masses of 0.1, 0.2, 0.3, 0.5, 1, 1.5, 2.0, and 2.5 $M_\odot$. The dashed lines show the D'Antona & Mazzitelli isochrones for 1×10^5 yr, 3×10^5 yr, 1×10^6 yr, 3×10^6 yr, 1×10^7 yr, and 3×10^7 yr. The HR diagram positions of T Tauri stars in the Taurus-Auriga molecular cloud, segregated between weak-emission (WTTS) and strong-emission (CTTS) stars, are taken from Kenyon & Hartmann (1995). (a) The upper heavy solid line corresponds to birthline accretion rate of $\dot{M}_b = 2 \times 10^{-6} M_\odot\,\mathrm{yr}^{-1}$. The lower heavy solid lines show post-birthline evolutionary tracks for zero accretion (connected by solid triangles) and for $\dot{M} = 10^{-7} M_\odot\,\mathrm{yr}^{-1}$ (open triangles). The triangles mark the positions of stars of 0.3, 0.5, and $1.0 M_\odot$ at elapsed times after the end of birthline accretion of 3×10^5, 1×10^6, and 3×10^6 yr. Post-birthline stars may initially move slighly above their birthline positions before descending in the HR diagram (see text).

thermal envelope emission accounts for the weakness of 2.3μm CO first-overtone absorption lines in protostellar sources (Casali & Eiroa 1996). Disk emission alone is unlikely to explain the observed effect, either because disks exhibit their own CO absorption, or because inner disk holes eliminate the region of the disk which can emit in the near infrared. We find that this near infrared veiling is very dependent on the envelope density, increasing as mass infall rate increases and centrifugal radius decreases. The veiling also depends on the characteristics of the underlying object and it is largest when most of the luminosity is due to accretion and the disk hole size is several stellar radii. The observed veiling indicates that dust must be falling in to distances of ~ 0.1 AU of the central star.

MAGNETOSPHERIC ACCRETION MODELS FOR THE HYDROGEN EMISSION LINES OF T TAURI STARS

Calvet and a student at UMass, J. Muzerolle, have developed a multilevel atom, 3D radiative transfer code applicable to arbitrary geometries and velocity fields, adopting the Sobolev approximation. This new development is based on the code CV by R. Hewett, which was restricted to a two-level atom approximation. Using this code, line fluxes and profiles have been calculated for optical and infrared emission lines for a grid of models covering a range of mass infall rates, temperatures, and emitting region sizes. The goals of this work are: (1) to determine mass infall rates for stars in T Taurus and compare the results with determinations from other indicators (i.e., continuum veiling); (2) to find indicators of mass infall rate, temperature, and size, for application to stars in distant/embedded clusters.

The first results of this effort were presented in a paper to appear in the Astrophysical Journal (Muzzerole, Calvet, & Hartmann 1997). Using a statistical equilibrium radiative transfer treatment, we examined the behavior of hydrogen emission lines arising from the magnetospheric infall zones of classical T Tauri stars. Having calculated self-consistent line profiles of the Balmer lines, Paβ and Brγ, we explored parameter space, examining the effects of the magnetospheric gas temperature and size on the line fluxes (see Figure 7). We compared model and observed line fluxes for the Balmer lines, and found a good match using a relatively small range of parameters.

Unfortunately, relatively few infrared line fluxes for other young stellar objects have been published, and then only for YSOs with the highest accretion rates. However, high-resolution line *profiles* have been recently obtained, most notably in Najita et al. (1996 - hereafter, NCT) and Folha et al. (1997); thus, we can at least compare observed and model line profiles, if not fluxes. Figure 8 compares an observed high-resolution line profile of Brγ from NCT to a model profile with typical CTTS parameters. The match to the WL 16 Brγ profile is of special interest, since the source is an embedded object. Determinations of the accretion rate of such objects using the standard veiling techniques are impossible due to the large extinction. We estimate the accretion rate by assuming the bolometric luminosity of WL 16 is due entirely to accretion, and obtain a value of about $10^{-5.5}\ M_\odot\, yr^{-1}$ (again, using standard TTS parameters). Our match to the observed profile uses an accretion rate of $10^{-6}\ M_\odot\, yr^{-1}$, and has a total line flux fairly similar to the value determined by NCT (about $2.4 \times 10^6\ erg\, cm^{-2}\, s^{-1}$). The model line is somewhat narrower than the observed profile; we are currently exploring models with a higher-mass star (NCT estimates a value of about $2.5 M_\odot$ for WL 16), which should increase the linewidth since the gas infall velocities will increase.

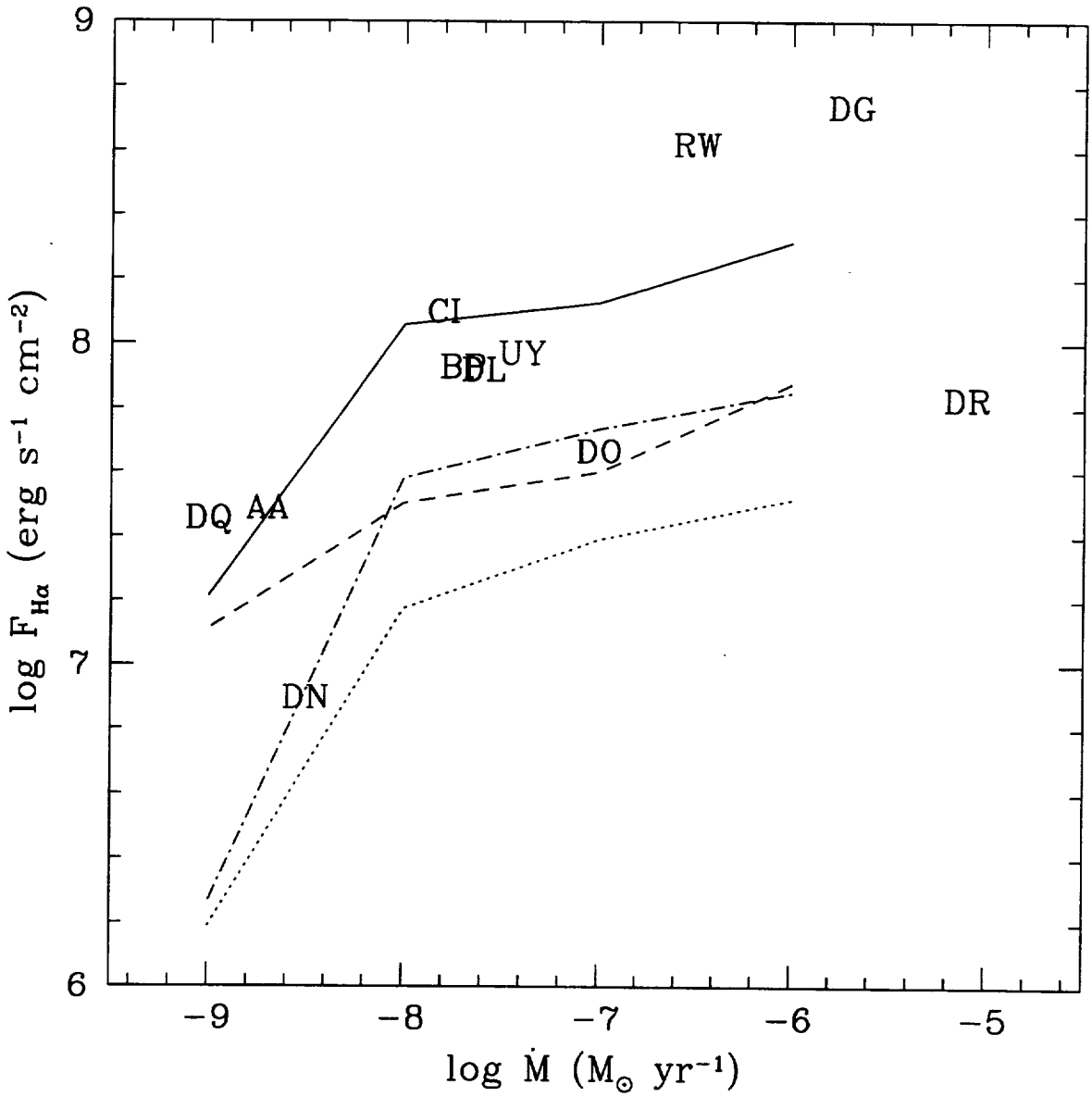

Figure 2: Integrated Hα line flux versus accretion rate for selected CTTS in Taurus. Observed data are delineated by the first two letters of the star name. Line fluxes are from Kuhi (1974), dereddened with A_V from GHBC except: DL, CI, and RW Tau, from VBJ; DR and DG Tau, from HEG. Accretion rates from GHBC, with the same exceptions (see text). All models have $M_* = 0.5\ M_\odot$, $R_* = 2\ R_\odot$. *Dotted line*, $r_{mi} = 2.2\ R_*$, $r_{mo} = 3\ R_*$, $T_{max} = 8000\ K$; *dash-dotted line*, $r_{mi} = 4\ R_*$, $r_{mo} = 6\ R_*$, $T_{max} = 8000\ K$; *dashed line*, $r_{mi} = 2.2\ R_*$, $r_{mo} = 3\ R_*$, $T_{max} = 10,000\ K$; *solid line*, $r_{mi} = 4\ R_*$, $r_{mo} = 6\ R_*$, $T_{max} = 10,000\ K$.

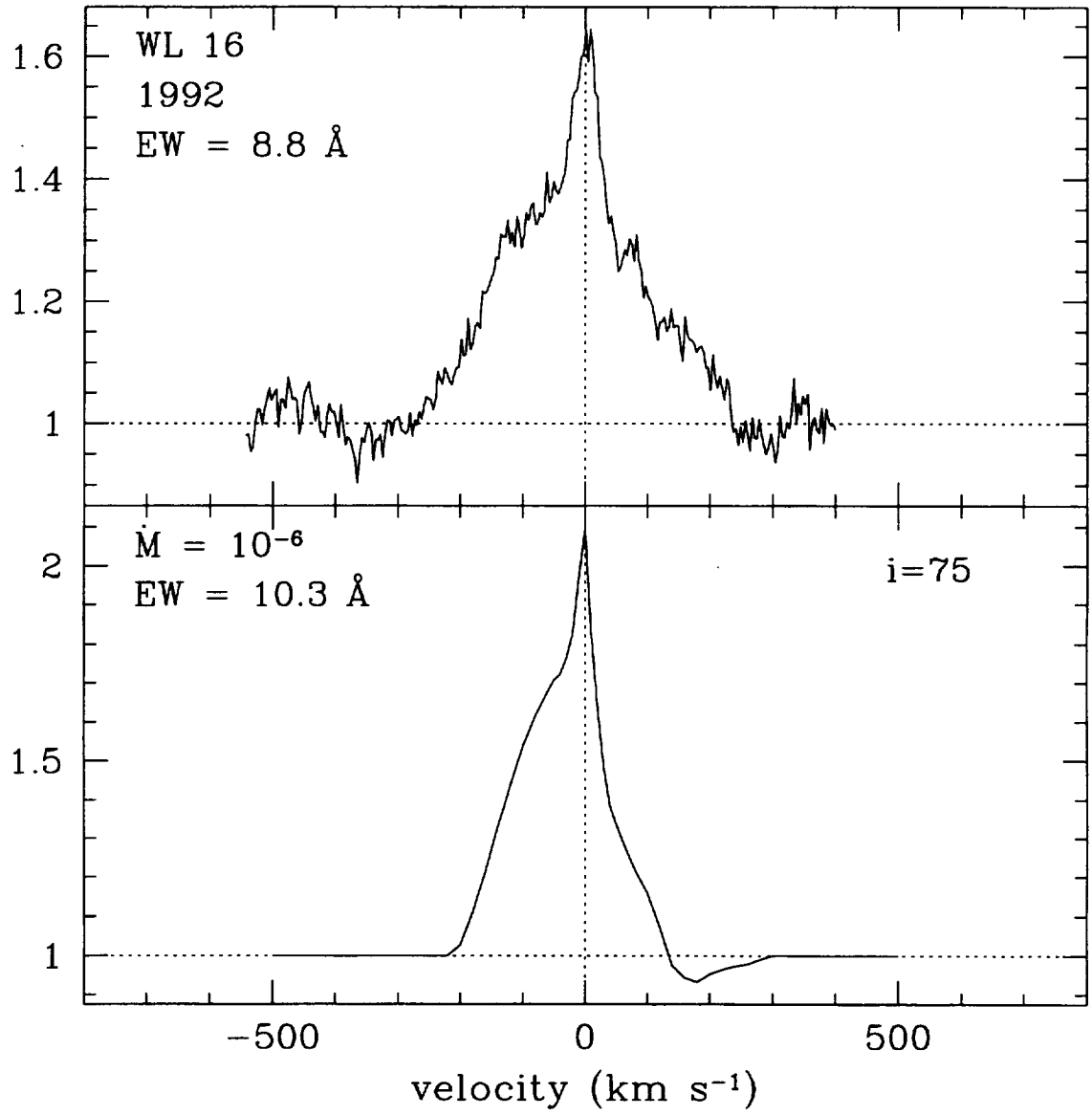

Figure 3: Comparison of model Brγ profile with observed profile for the embedded object WL 16 from Najita et al. (1996).

This result is encouraging in light of our goal of applying the magnetospheric accretion models to infer mass accretion rates in heavily-extincted YSOs, although the line thermalization problem found in the Balmer lines is also present (albeit to a lesser degree) in Brγ, and thus this line may not prove to be a useful accretion rate indicator. We have begun a project to study lines in the red region of the spectrum (the Ca II infrared triplet, the O I permitted lines) which may also be detected in objects of (relatively high) extinction. Our initial goal is to determine line fluxes for lightly extincted objects which already have independent measures of mass accretion rates, to see whether an *empirical* calibration of $\dot{M}$ and line fluxes can be established. We will then follow this up with theoretical modelling to see if we can understand the observed trends. Preliminary results suggest that, at least at an approximate level, the fluxes of the Ca II lines can be used to distinguish between high, medium, and low mass accretion rates ($\sim 10^{-7}$, 10^{-8}, and $10^{-9} M_{\odot} yr^{-1}$).

References

Note: * indicates publication supported by this grant

Adams, F.C., Lada, C.J., & Shu, F.H. 1987, ApJ, 312, 788

Andre, P., Ward-Thompson, D., & Barsony, M. 1993, APJ, 406 122

Beckwith, S.V.W., & Birk, C.C. 1995, ApJ, 449, L59

* Calvet, N., Hartmann, L., Kenyon, S., & Whitney, B. 1994, ApJ, 434, 330

* Calvet, N., Hartmann, L., & Strom, S. 1997, ApJ, 481, 912

Casali, M.M., & Eiroa, C. 1996, A&A, 306, 427

Cassen, P., & Moosman, A. 1981, Icarus, 48, 353

Chick, K.M., Pollack, J.B., & Cassen, P. 1995, ApJ, submitted

* D'Alessio, P., Calvet, N., & Hartmann, L. 1997, ApJ, in press

Gahm, G.F., Loden, K., Gullbring, E., and Hartstein, S. 1995, AA, 301, 89

Gledhill, T.M., & Scarrott, S.M. 1989, MNRAS, 236, 139

Grasdalen, G.L., Sloan, G., Stout, M., Strom, S.E., & Welty, A.D. 1989, ApJL, 339, L37

* Hartmann, L., Boss, A.P., Calvet, N., & Whitney, B. 1994, ApJL, 430, L49

* Hartmann, L., Calvet, N., & Boss, A.P. 1996, ApJ, 464, 387

* Hartmann, L., Cassen, P., & Kenyon, S. 1997, ApJ, 475, 770

Hayashi, M., Ohashi, N., & Miyama, S. 1993, ApJ, 418, L71

* Kenyon, S.J., Calvet, N., & Hartmann, L. 1993a, ApJ, 414, 676

* Kenyon, S.J., & Hartmann, L. 1995, ApJS, 101, 117

* Kenyon, S.J., Whitney, B., Gomez, M., & Hartmann, L. 1993b, ApJ, 414, 773

Lay, O.P., Carlstrom, J.E., Hills, R.E., & Phillips, T.G. 1994, ApJ, 434, L75

Myers, P.C., Fuller, G.A., Goodman, A.A., & Benson, P.J. 1991, ApJ, 376, 561

Nakamura, F., Hanawa, T., & Nakano, T. 1995, ApJ, 444, 770

Palla, F., & Stahler, S.W. 1992, ApJ, 392, 667

Sargent, A.I., & Beckwith, S. 1991, ApJ, 382, L31

Shu, F.H. 1977, ApJ, 214, 488

Stahler, S.W. 1988, ApJ, 332, 804

Stapelfeldt, K.R., Burrows, C.J., Krist, J.E., Trauger, J.T., Hester, J.J., Holtzman, J.A., Ballester, G.E., Casertano, S., Clarke, J.T., Cristp, D., Evans, R.W., Gallagher, J.S. III, Griffiths, R.E., Hoessel, J.G., Mould, J.R., Scowen, P.A., Watson, A.M., & Westphal, J.A. 1995, ApJ, L Aug 20.

Weintraub, D.A., Kastner, J.H., & Whitney, B.A. 1995, preprint

Whitney, B. A., & Hartmann, L. 1993, ApJ, 402, 605

INFALLING ENVELOPES AND PRE-MAIN SEQUENCE DISKS

Final Report 11/01/90 - 9/30/97, NAGW-2306, Hartmann et al.

The goal of this project has been to understand the observed infrared emission of young stellar objects, and explore the implications of this emission for the evolution of dusty envelopes and circumstellar disks. We are using sophisticated radiative transfer methods to compare models with observations, thereby making critical tests of the standard picture of low-mass star formation. This grant period is a combination of two three-year grants under the same number.

THERMAL EMISSION FROM PROTOSTELLAR ENVELOPES

Our initial project was to study the infrared spectra of protostellar or Class I sources, such as shown in the leftmost panel of Figure 1. We showed that much of the infrared emission of Class I sources in the Taurus-Auriga molecular cloud could be reproduced by the dusty rotating collapse models developed by Terebey, Shu, & Cassen (1984). By allowing the stellar luminosity to be a free parameter, and correctly accounting for the inclination-dependent extinction through the infalling envelope, we found that typical Taurus Class I sources have infall rates similar to those predicted by simple theory (Shu 1977), and have sufficient rotation that material is falling onto circumstellar disks out to radii ~ 70 AU from the central star (Kenyon *et al.* 1993a,b).

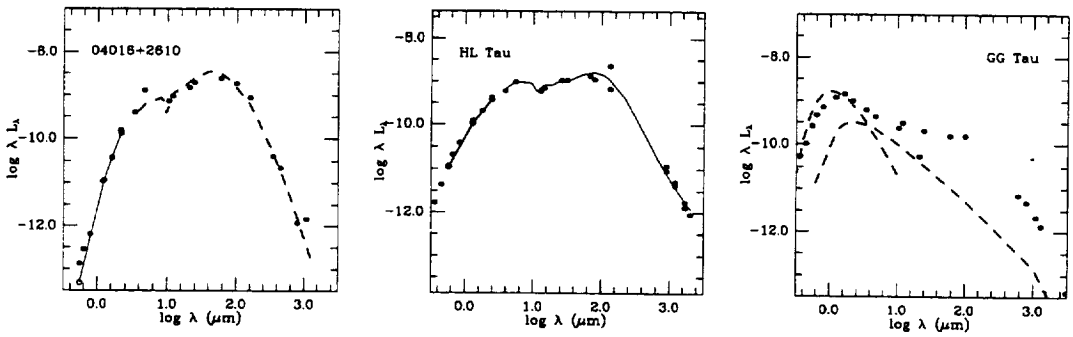

Figure 1: Left panel: Comparison of radiative transfer models of infalling envelopes (dashed lines, open circles) with observed fluxes for the protostellar source IRAS 04016+2610. Center panel: comparison of the spectral energy distribution of the flat-spectrum source HL Tau with a similar infall model, with the same mass infall rate as in the left panel, but somewhat larger rotation. *Right panel*: the spectral energy distribution of a typical T Tauri star, compared with the expected emission from a blackbody and simple disk model (dashed lines). From Calvet *et al.* (1994).

Next we studied the "flat spectrum" T Tauri stars, such as HL Tau (middle panel of Figure 1). The infrared emission from flat-spectrum T Tauri stars had been interpreted as arising from a relatively hot disk with a temperature distribution $T \propto r^{-1/2}$ that was not theoretically understood (Adams *et al.* 1988; Beckwith *et al.* 1990). However, it is apparent from Figure 1 that the infrared

emission from flat spectrum sources is similar to that of infall sources. We were able to show (Calvet *et al.* 1994) that flat-spectrum sources could indeed be understood as objects with substantial infalling envelopes. Flat spectrum sources are really protostars, either viewed roughly along some sort of hole or path of lower extinction in the envelope, or objects in which the infall phase is coming to an end, reducing the extinction through the envelope. Our results explained the flat spectrum without requiring any unusual physics - just simple radiative transfer in a freely-infalling dusty cloud (see Figure 1). The far-infrared emission of flat spectrum sources arises in the envelope, not the disk, and so this emission cannot be used to constrain disk properties.

Our final goal was originally to try to understand the infrared emission of typical T Tauri stars, such as that of GG Tau in the rightmost panel of Figure 1. We thought that the observed excess far-infrared emission, which is not simply explainable in terms of simple steady flat disk theory, might be explained by infall of a remnant, tenuous dusty envelope, by analogy with the results for the flat-spectrum sources. If this idea is correct, the implications for circumstellar disk evolution are important; even a very small infall rate of $\sim 10^{-8} M_\odot\ yr^{-1}$, more than two orders of magnitude smaller than the collapse rate in the main infall phase, could add a "minimum-mass" solar nebula over a typical T Tauri lifetime of 10^6 yr.

But before addressing this possibility, it became clear that we needed to investigate additional departures from spherical symmetry in infalling envelopes beyond the effects of rotation in the TSC model. Real young stellar objects clearly have non-spherically-symmetric envelopes, as made evident in observations of scattered light nebulae, and cannot be explained with Terebey *et al.* (1984) infall models. The question then arises, how reliable are our estimates of envelope parameters such as infall rates and the envelope angular momentum, and is our interpretation of flat-spectrum sources materially altered?

To explore these issues, we first considered envelopes in which the strong departure from spherical symmetry is caused by an outflow, which carves a cavity in the dusty infalling envelope (Whitney & Hartmann 1993; Kenyon *et al.* 1993b). Although this model was able to explain the observed morphology and colors of scattered light nebulae in the optical and near-infrared spectral regions (Kenyon *et al.* 1993b), wide-angle outflows cause serious difficulties for understanding spectral energy distributions (Calvet *et al.* 1994). The reason is simply that an outflow which has a substantial opening angle removes all of the low-angular momentum material falling in, and therefore eliminates the mid-infrared emission from the model.

SHEET MODELS OF PROTOSTELLAR COLLAPSE

Observations (Myers et al. 1991) indicate that protostellar molecular cloud cores are not spherically symmetric, but are noticably elongated. To investigate the potential effects of initial protostellar cloud geometry on collpase, in a previous paper supported by this grant (Hartmann *et al.* 1994) we presented an initial exploration of protostellar collapse from a flattened cloud. We considered the time-dependent axisymmetric evolution of a marginally Jeans-unstable region in an isothermal, non-magnetic, non-rotating, self-gravitating sheet. An important aspect of collapse from a sheet, which differs qualitatively from contraction of an initially spherical distribution of material, is the appearance of two "bipolar" cavities on either side of the central plane of the sheet. The cavities result simply because the regions closest to the central mass fall in before material from distant regions in the plane of the sheet can reach the center. Similar infall cavities were

found in the simulations of the collapse of a rotating, magnetized filamentary cloud by Nakamura *et al.* (1995).

We published calculations aimed at addressing some of the observational consequences of the sheet collapse model (Hartmann, Calvet, & Boss 1996). To calculate the predicted emission from sheet collapse models in a reasonably accurate way, we needed to extend the results of Paper I to finer spatial grids near the central protostar than generally feasible with hydrodynamic calculations for the entire envelope. We also had to modify the results of Paper I to include rotation, because the angular momentum of the collapsing cloud plays a crucial role in determining the extinction through the inner envelope (see discussion in Adams *et al.* 1987). Our strategy is to assume that rotation plays a small role at large scales, as also assumed in the TSC solutions, so that we can use the results of Paper I to calibrate our large-scale density structure, while modifying the solution on small scales to account for the angular momentum barrier. Here we develop an analytic model which accounts for rotation and can also be divided into a sufficiently fine spatial grid for the calculation of the inner envelope emission.

Figure 2 compares the simulation in Paper I at one point in time with the analytic sheet collapse models. The overall properties of the density distribution are approximately reproduced with the appropriate choice of the parameter η. The agreement is reasonable, especially when one considers that this solution is really only valid for regions much smaller than than the outer cloud radius. The model works better at later times than at earlier times, partly because there are substantial departures from radial free-fall motions during the initial stages of collapse.

Figure 3 shows J band (1.25μm) images and polarization patterns for sheet models with the above parameters and $\eta = 1, 2, 3, 4$, viewed at an inclination of $i = 60°$ to the line of sight. The images have been convolved with a gaussian point spread function with a full-width at half-maximum of one pixel (= 28 AU) to smooth the results slightly.

These images show that the sheet collapse models naturally produce reflection nebulae which appear to have large opening angles. As discussed in §3.2, values of $\eta \sim 2.5 - 3.5$ are characteristic of the envelope density distribution during the main infall phase, which would produce very open cavities. Since η should increase with increasing time, the sequence shown in Figure 5 corresponds to a time sequence, suggesting that the opening angle of reflection nebulae should increase with increasing age. The polarization patterns are generally centrosymmetric, with some departures near the highest extinction regions from multiple scattering (Whitney & Hartmann 1993).

Our results suggest that collapse cavities can naturally explain the morphological appearance of many reflection nebulae around young stars on small distance scales without requiring initially diverging outflows. Sheet collapse models can simultaneously explain small-scale reflection nebula morphologies and dust envelope emission properties of many young stellar objects more easily than the standard spherical collapse models. The sheet collapse picture suggests that protostars, i.e. young stellar objects still accreting a large fraction of their mass from infalling envelopes, may be optically visible over a substantial range of system inclinations to the line of sight. These results may be especially relevant to cases where fragmentation and collapse has been triggered by an external impulse, such as a shock wave.

As another example of how sheet infall models can eliminate the discrepancy between SED fitting and the reflection nebula morphology, we applied our models to the flat spectrum T Tauri star HL Tau. This optically-visible object has a very large infrared excess, so that the SED is relatively flat between about 3 and 100 μm. Calvet *et al.* (1994) showed that the mid- to far-infrared emission of HL Tau could be reproduced by infalling envelope models with typical parameters of

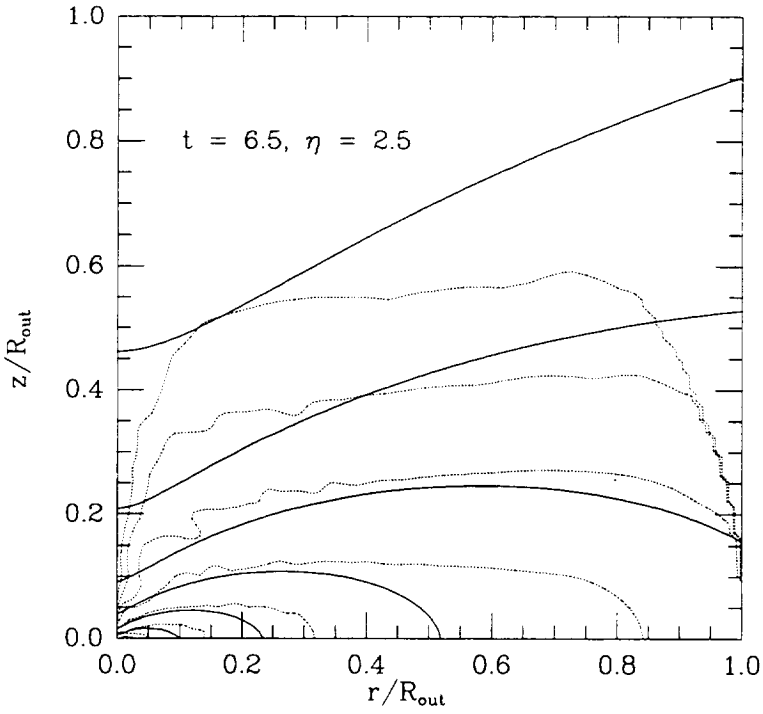

Figure 2: Comparison between the density distributions of the numerical simulation and sheet models. The spatial dimensions are given in units of the outer radius of the cloud $R_{out} = 8.6 \times 10^{16}$ cm. The numerical density distribution at at a time of 6.5 free-fall times $= 3 \times 10^5$ yr is compared with the density distribution of a sheet model characterized by a mass infall rate $6 \times 10^{-6} M_{\odot} yr^{-1}$, a central mass of $0.21 M_{\odot}$ (half that of the central mass in the numerical simulation), and $\eta = 2.5$. The lowest density contour corresponds to a molecular hydrogen number density of $10^4 cm^{-3}$, and subsequent contours represent factors of $10^{1/2}$ increase in density.

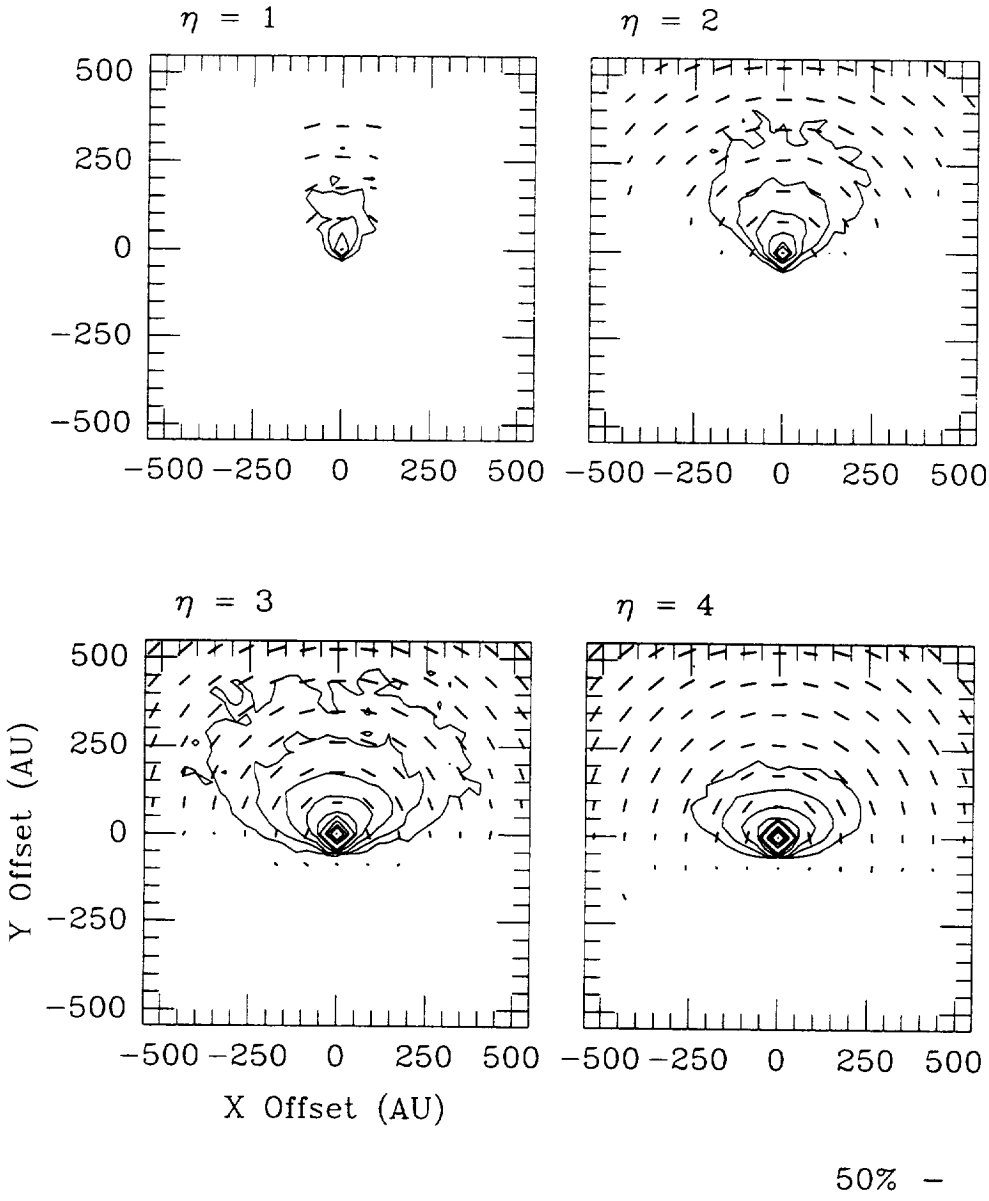

Figure 3: Images and polarization maps at 1.25μm, $i = 60°$, for the $\eta = 1, 2, 3, 4$ models with $\dot{M} = 4 \times 10^{-6} M_{\odot} yr^{-1}$, $R_c = 50$ AU, and $M = 0.5 M_{\odot}$, assuming MRN dust parameters. The opening angle of the reflection nebula increases with increasing η.

Class I stars in Taurus; in particular, the SEDs of 04016+2610 and HL Tau are very similar. The infall rate needed to explain the far-infrared emission is also consistent with analyses of near-infrared scattered light by Beckwith *et al.* (1989), redshifted C_2 absorption (Grasdalen *et al.* 1989), and ^{13}CO radio interferometer maps (Hayashi *et al.* 1993). However, as in the case of 04016+2610, the Calvet *et al.* envelope model for the SED HL Tau was unsatisfactory in that it demanded a narrow polar envelope hole, with a half-angle $\sim 10°$. In contrast, the observed optical nebula has a quite large apparent opening half-angle, $\approx 45°$ (e.g., Gledhill & Scarrott 1989; Stapelfeldt *et al.* 1995), but a cavity model with a streamline hole, adopting an opening angle of this magnitude, would result in an unacceptable fit to the SED.

We showed that sheet collapse models can explain the SED, the scattered light image, and the near-infrared polarization and photocenter shift with wavelength in HL Tau. Our constraints are (1) an infall rate comparable to that derived by Hayashi *et al.* (1993) from independent analysis of the ^{13}CO interferometer maps, and (2) a centrifugal radius R_c smaller than the ~ 140 AU outer disk radius suggested by the sub-mm interferometry of Lay *et al.* (1994). (We expect that the disk, if anything, will have spread to larger radii than R_c; Cassen & Moosman 1981). The first constraint is straightforwardly met, since we assume $\dot{M} = 4 \times 10^{-6} M_\odot yr^{-1}$, the typical mean value of infall rates found for Taurus Class I sources by Kenyon *et al.* (1993a), essentially equal to the infall rate derived by Hayashi *et al.* (1993), and sufficiently close to the $\dot{M} \sim 6 \times 10^{-6} M_\odot yr^{-1}$ we found for the "plateau" phase of infall in our isothermal numerical simulation. We also adopt $R_c = 50$ AU for concreteness, although the precise value adopted is not critical given the sensitivity of the results to inclination. Finally, since HL Tau is apparently surrounded by an envelope with a mass accretion rate comparable to that observed and predicted for the main infall phase, we might expect "intermediate" values of $\eta \sim 2 - 3$.

Figure 4 compares SEDs calculated for sheet collapse models with $\eta = 2, 3$ to the observed SED of HL Tau. The $\eta = 2$ model fits the long-wavelength infrared emission better than the $\eta = 3$ model, which exhibits too much flux. Once again we emphasize that our assumption of a spherical temperature distribution may cause the comparison with the $\eta = 3$ model to appear worse than it actually should. In a more accurate radiative equilibrium calculation, the polar, low density, regions will be hotter because radiation will preferentially escape in these directions; the equatorial, densest regions, will become cooler. Since the far infrared emission comes from optically-thin regions, and most of the emitting envelope in a sheet model is in the equatorial region, a sheet model would probably have lower temperatures and therefore lower far-infrared fluxes. This conjecture is supported by the modelling of Chick *et al.* (1995), who considered infalling envelopes with cavities; using a Rosseland mean opacity, Chick *et al.* found that the equatorial envelope temperatures could be as much as a factor of two lower than the spherical case for large cavities, such as implicit in the $\eta = 3$ model.

We also showed that the depth of the 10μm silicate feature is very sensitive to the system inclination. In both models the best comparisons occur for $i \sim 65°$, or $\mu \sim 0.4$. Our models show that the silicate feature depth is so geometry-dependent that it is unlikely to be a reliable measure of envelope optical depth.

Figure 5 shows scattered light images for the $\eta = 2, 3$ models at appropriate inclinations. The observed HL Tau J-band polarization can be reproduced at $\eta = 2$ if $\mu = 0.5$ or at $\eta = 3$ if $\mu = 0.3$. The true system inclination is unknown, but the aspect ratio of the molecular gas observed by Sargent & Beckwith (1991) and Hayashi *et al.* (1993) suggests $\mu \approx 0.5$. The appearance of the large-scale scattered light nebula is perhaps better matched by $\eta = 3$ models, which provide

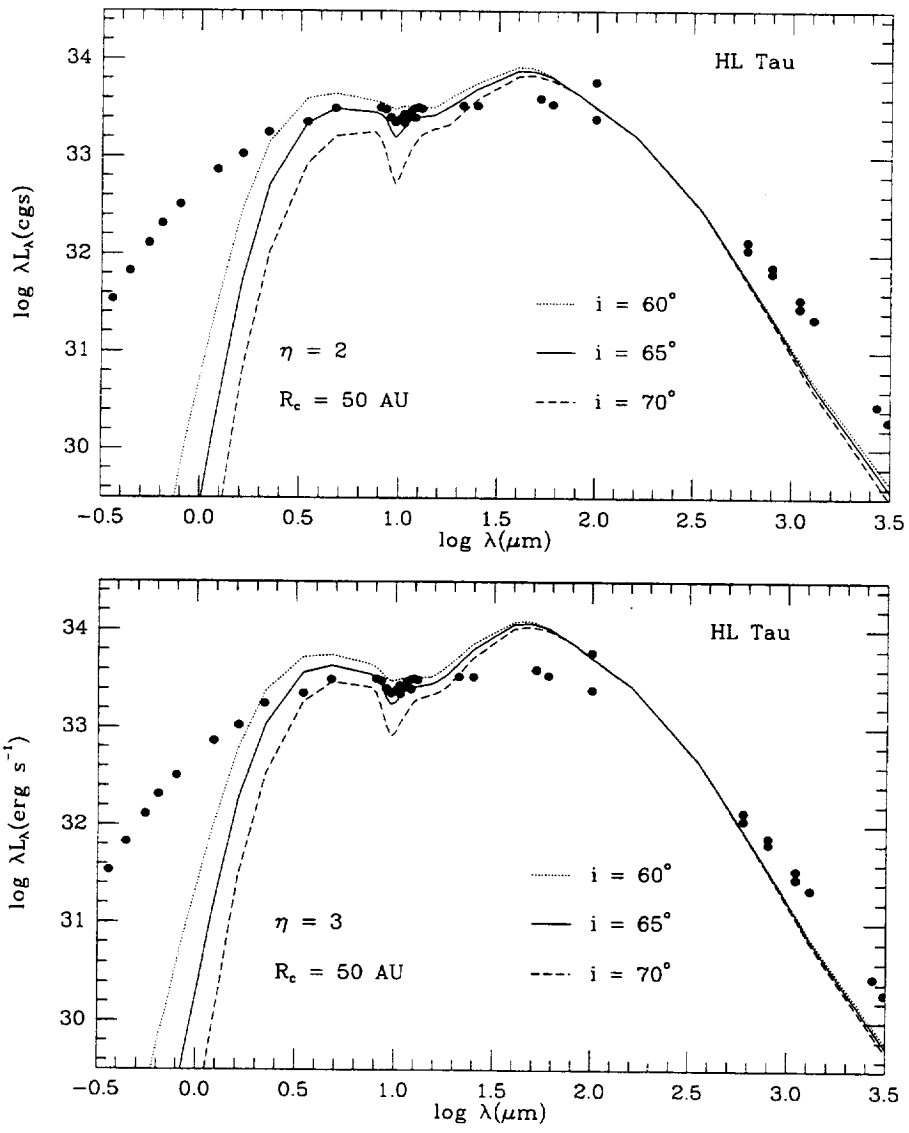

Figure 4: Spectral energy distribution of the flat-spectrum T Tauri star HL Tau (Calvet *et al.* 1994), compared with flattened collapse models with $\eta = 2, 3$ and $R_c = 50$ AU.

reasonable agreement with the wide opening angle suggested by large-scale images, although the HST images show fine-scale structure in the nebula (Stapelfeldt *et al.* 1995) that cannot possibly be explained by the simple axisymmetric model used here.

The Calvet *et al.* spherical collapse model for HL Tau demanded a narrow outflow hole, because an evacuated hole with a wide opening angle eliminates the mid-infrared excess as discussed above (see also Figure 6 of Calvet *et al.* 1994). With such a narrow cavity, the reflection nebula morphology would look quite different than observed. The η models do not have the same problem because the envelope cavity is not completely evacuated of dust; even small amounts of material can provide the required mid-infrared emission.

Beckwith & Birk (1995) showed that the position of the peak near-infrared intensity in HL Tau shifts in position by about $0.53 \pm 0.07 \, arcsec \sim 74$ AU between 2.12 μm and 1.25 μm; this result was confirmed and extended in wavelength by Weintraub, Kastner, and Whitney (1995). Both sets of authors interpret this shift as due to a combination of an extended scattered light nebula seen behind a medium with an extinction gradient. Beckwith & Birk suggested that the extincting medium might be either an infalling envelope or the extended atmosphere of a circumstellar disk; Weintraub *et al.* favored the former explanation.

Our models also predict photocenter shifts, since the central star is hidden by a scattering, absorbing envelope with a substantial spatial gradient in its column density. We convolved the models with a $1 \, arcsec$ gaussian point spread function to be more directly comparable to the ground-based measurements. For $\eta = 2$, we find shifts at J of 16 AU and 53 AU at $\mu = 0.5$ and $\mu = 0.4$, respectively; for $\eta = 3$, the shifts at J are 10 AU and 63 AU at $\mu = 0.4$ and $\mu = 0.3$, respectively. The two largest of these shifts are reasonably consistent with the observations, although the polarizations predicted by the large photocenter shift models, 11% and 19%, are somewhat larger than observed.

Thus, in general our models were quite successful in explaining many observed features of protostellar sources. Since protostellar clouds are not spherically-symmetric, our results should be generally applicable to such sources.

THE STRUCTURE AND EMISSION OF ACCRETION DISKS IRRADIATED BY INFALLING ENVELOPES

In a recently accepted paper (D'Alessio et al. 1997) we calculated the emission from steady viscous disks heated by radiation from an opaque infalling protostellar envelope. For typical envelope parameters used to explain the spectral energy distributions of protostellar sources, we found that the envelope heating raises the outer disk temperature dramatically. The resulting temperature distribution in the disk is a complicated function of both radial distance and vertical height above the disk midplane. We showed that the visibility flux at $\lambda = 0.87 \, mm$ and the spectral energy distribution from submm to radio wavelengths of the flat-spectrum T Tauri star HL Tau can be explained by emission from an accretion disk irradiated by its infalling envelope, whereas thermal emission from an infalling envelope or radiation from a steady viscous accretion disk cannot explain the observations. Our results suggest that the radiation fields of collapsing protostellar envelopes may strongly affect the structure of pre-main sequence accretion disks.

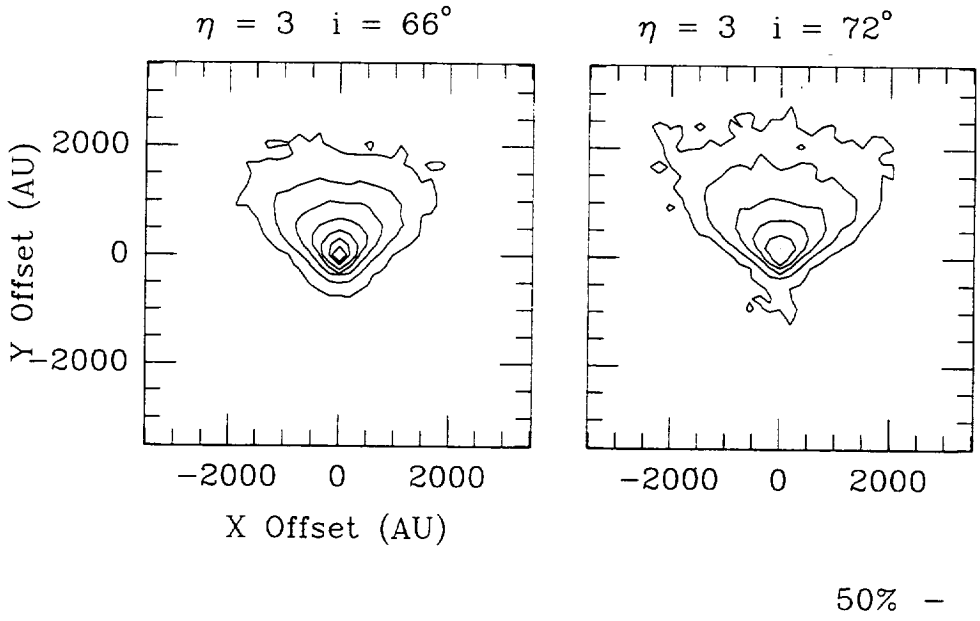

Figure 5: Scattered light calculations at $\lambda = 1.25\mu$ for $\eta = 2, 3$, each at two inclinations, for the HL Tau models.

DISK ACCRETION AND THE STELLAR BIRTHLINE

In Hartmann, Cassen, & Kenyon (1997), we presented a simplified analysis of some effects of disk accretion on the early evolution of fully-convective, low-mass pre-main sequence stars. Our analysis builds on the previous seminal work of Stahler (1988) but differs in that the accretion of material occurs over a small area of the stellar surface, such as through a disk or magnetospheric accretion column, so that most of the stellar photosphere is free to radiate to space. This boundary condition is similar to the limiting case considered by Palla & Stahler (1992) for intermediate-mass stars.

We argued that for a wide variety of disk mass accretion rates, material will be added to the star with relatively small amounts of thermal energy. Protostellar evolution calculated assuming this "low-temperature" limit of accretion generally follows the results of Stahler because of the thermostatic nature of deuterium fusion, which prevents protostars from contracting below a "birthline" in the HR diagram. Our calculated protostellar radii tend to fall below Stahler's at higher masses; the additional energy loss from the stellar photosphere in the case of disk accretion tends to make the protostar contract. The low-temperature disk accretion evolutionary tracks never fall below the deuterium-fusion birthline until the internal deuterium is depleted, but protostellar tracks can lie above the birthline in the HR diagram if the initial radius of the protostellar core is large enough, or if rapid disk accretion (such as might occur during FU Ori outbursts) adds significant amounts of thermal energy to the star. These possibilities cannot be ruled out by either theoretical arguments or observational constraints at present, so that individual protostars might evolve along a multiplicity of birthlines with a modest range of luminosity at a given mass.

Our results indicate that there are large uncertainties in assigning ages for the youngest stars from HR diagram positions, given the uncertainty in birthline positions. Our calculations also suggest that the relatively low disk accretion rates characteristic of T Tauri stars below the birthline cause low-mass stars to contract only slightly faster than normal Hayashi track evolution (Figure 5), so that ages for older pre-main sequence stars estimated from HR diagram positions are relatively secure.

NEAR-INFRARED EMISSION OF PROTOSTARS

In Calvet, Hartmann, & Strom (1997), we presented models for the thermal emission from dusty infalling envelopes around protostars, which indicate that the envelope emission can greatly exceed the stellar + disk photospheric emission at wavelengths $\sim 2\mu$m. We argued that this thermal envelope emission accounts for the weakness of 2.3μm CO first-overtone absorption lines in protostellar sources (Casali & Eiroa 1996). Disk emission alone is unlikely to explain the observed effect, either because disks exhibit their own CO absorption, or because inner disk holes eliminate the region of the disk which can emit in the near infrared. We find that this near infrared veiling is very dependent on the envelope density, increasing as mass infall rate increases and centrifugal radius decreases. The veiling also depends on the characteristics of the underlying object and it is largest when most of the luminosity is due to accretion and the disk hole size is several stellar radii. The observed veiling indicates that dust must be falling in to distances of ~ 0.1 AU of the central star.

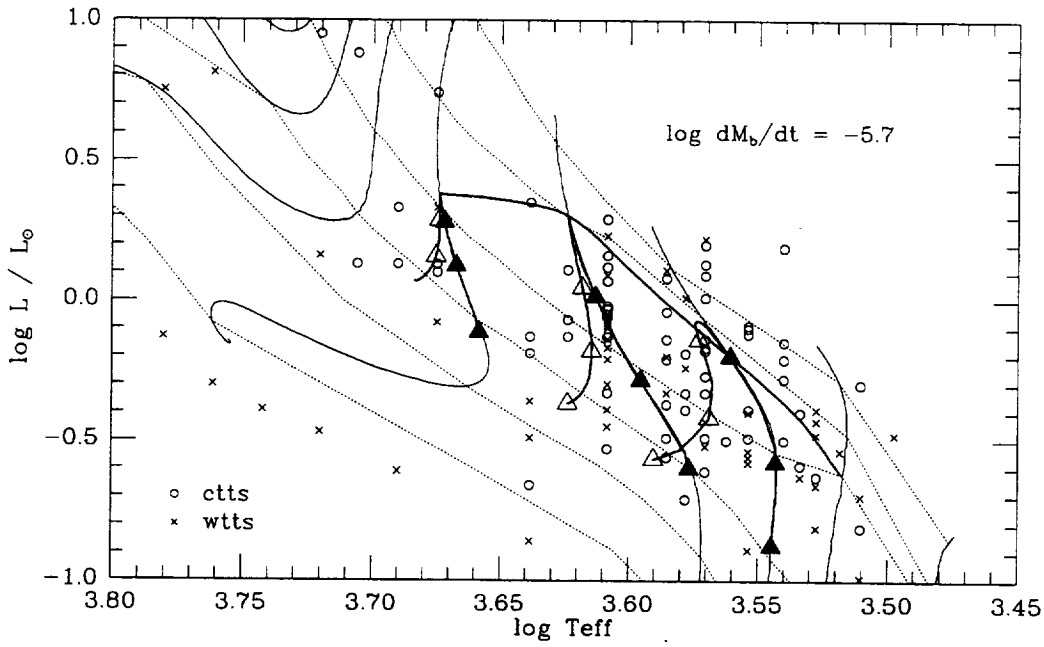

Figure 6: Stellar evolutionary tracks for low-temperature ($\alpha = 0$) disk accretion, compared with observations of T Tauri stars in the Taurus-Auriga star forming region. The evolutionary tracks are calculated interpolating in the CMA results to provide the calibration of $L_{phot}(M, R)$, producing small departures from the power-law calibration results shown in previous figures. The light solid lines show the pre-main sequence evolutionary tracks of D'Antona & Mazzitelli for masses of 0.1, 0.2, 0.3, 0.5, 1, 1.5, 2.0, and 2.5 $M_\odot$. The dashed lines show the D'Antona & Mazzitelli isochrones for 1×10^5 yr, 3×10^5 yr, 1×10^6 yr, 3×10^6 yr, 1×10^7 yr, and 3×10^7 yr. The HR diagram positions of T Tauri stars in the Taurus-Auriga molecular cloud, segregated between weak-emission (WTTS) and strong-emission (CTTS) stars, are taken from Kenyon & Hartmann (1995). (a) The upper heavy solid line corresponds to birthline accretion rate of $\dot{M}_b = 2 \times 10^{-6} M_\odot\,\mathrm{yr}^{-1}$. The lower heavy solid lines show post-birthline evolutionary tracks for zero accretion (connected by solid triangles) and for $\dot{M} = 10^{-7} M_\odot\,\mathrm{yr}^{-1}$ (open triangles). The triangles mark the positions of stars of 0.3, 0.5, and $1.0 M_\odot$ at elapsed times after the end of birthline accretion of 3×10^5, 1×10^6, and 3×10^6 yr. Post-birthline stars may initially move slighly above their birthline positions before descending in the HR diagram (see text).

MAGNETOSPHERIC ACCRETION MODELS FOR THE HYDROGEN EMISSION LINES OF T TAURI STARS

Calvet and a student at UMass, James Muzerolle, developed a multilevel atom, 3D radiative transfer code applicable to arbitrary geometries and velocity fields, adopting the Sobolev approximation. This new development is based on the code CV by R. Hewett, which was restricted to a two-level atom approximation. Using this code, line fluxes and profiles have been calculated for optical and infrared emission lines for a grid of models covering a range of mass infall rates, temperatures, and emitting region sizes. The goals of this work are: (1) to determine mass infall rates for stars in T Taurus and compare the results with determinations from other indicators (i.e., continuum veiling); (2) to find indicators of mass infall rate, temperature, and size, for application to stars in distant/embedded clusters.

The first results of this effort were presented in a paper to appear in the Astrophysical Journal (Muzzerole, Calvet, & Hartmann 1997). Using a statistical equilibrium radiative transfer treatment, we examined the behavior of hydrogen emission lines arising from the magnetospheric infall zones of classical T Tauri stars. Having calculated self-consistent line profiles of the Balmer lines, Paβ and Brγ, we explored parameter space, examining the effects of the magnetospheric gas temperature and size on the line fluxes (see Figure 7). We compared model and observed line fluxes for the Balmer lines, and found a good match using a relatively small range of parameters. We were also able to match the observed Brγ line profile of the embedded object WL 16, supporting the use of the infrared lines in studying magnetospheric infall even in the earliest stages of star formation. Finally, we discussed constraints on the physical parameters and the possibility of using the emission lines as accretion rate indicators.

We would like to compare model and observational results for the infrared lines. Unfortunately, relatively few line fluxes have been published, and then only for objects with the highest accretion rates. However, high-resolution line *profiles* have been recently obtained, most notably in Najita et al. (1996 - hereafter, NCT) and Folha et al. (1997); thus, we can at least compare observed and model line profiles, if not fluxes. Figure 8 compares an observed high-resolution line profile of Brγ from NCT to a model profile with typical CTTS parameters. The match to the WL 16 Brγ profile is of special interest, since the source is an embedded object. Determinations of the accretion rate of such objects using the standard veiling techniques are impossible due to the large extinction. We estimate the accretion rate by assuming the bolometric luminosity of WL 16 is due entirely to accretion, and obtain a value of about $10^{-5.5}\ M_\odot\, yr^{-1}$ (again, using standard TTS parameters). Our match to the observed profile uses an accretion rate of $10^{-6}\ M_\odot\, yr^{-1}$, and has a total line flux fairly similar to the value determined by NCT (about $2.4 \times 10^6\ erg\, cm^{-2}\, s^{-1}$). The model line is somewhat narrower than the observed profile; we are currently exploring models with a higher-mass star (NCT estimates a value of about $2.5 M_\odot$ for WL 16), which should increase the linewidth since the gas infall velocities will increase.

This result is encouraging in light of our goal of applying the model as a diagnostic tool for embedded CTTS, although the line thermalization problem we see in the Balmer lines is also present (albeit to a lesser degree) in Brγ, and thus this line may not prove to be a useful accretion rate indicator. However, more determinations of line fluxes for lightly extincted objects, over a wide range of accretion rates, are essential to establishing a possible accretion rate calibration with this line (or others, like Paβ). Nevertheless, a significant implication of this profile match is that magnetospheric accretion seems to occur at earlier evolutionary phases and in higher-mass objects than the classical T Tauri stars.

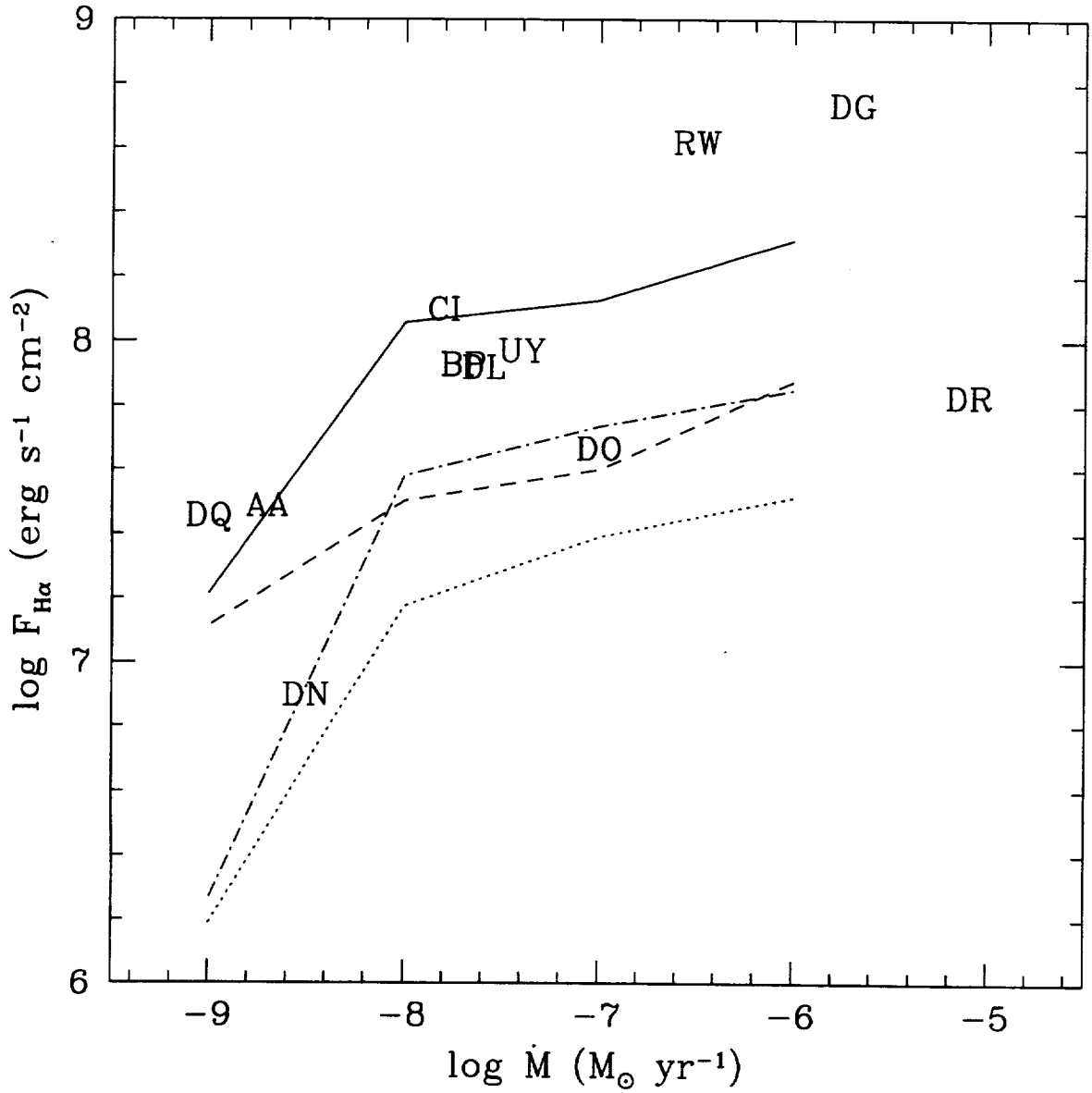

Figure 7: Integrated Hα line flux versus accretion rate for selected CTTS in Taurus. Observed data are delineated by the first two letters of the star name. Line fluxes are from Kuhi (1974), dereddened with A_V from GHBC except: DL, CI, and RW Tau, from VBJ; DR and DG Tau, from HEG. Accretion rates from GHBC, with the same exceptions (see text). All models have $M_* = 0.5\ M_\odot$, $R_* = 2\ R_\odot$. *Dotted line*, $r_{mi} = 2.2\ R_*$, $r_{mo} = 3\ R_*$, $T_{max} = 8000\ K$; *dash-dotted line*, $r_{mi} = 4\ R_*$, $r_{mo} = 6\ R_*$, $T_{max} = 8000\ K$; *dashed line*, $r_{mi} = 2.2\ R_*$, $r_{mo} = 3\ R_*$, $T_{max} = 10,000\ K$; *solid line*, $r_{mi} = 4\ R_*$, $r_{mo} = 6\ R_*$, $T_{max} = 10,000\ K$.

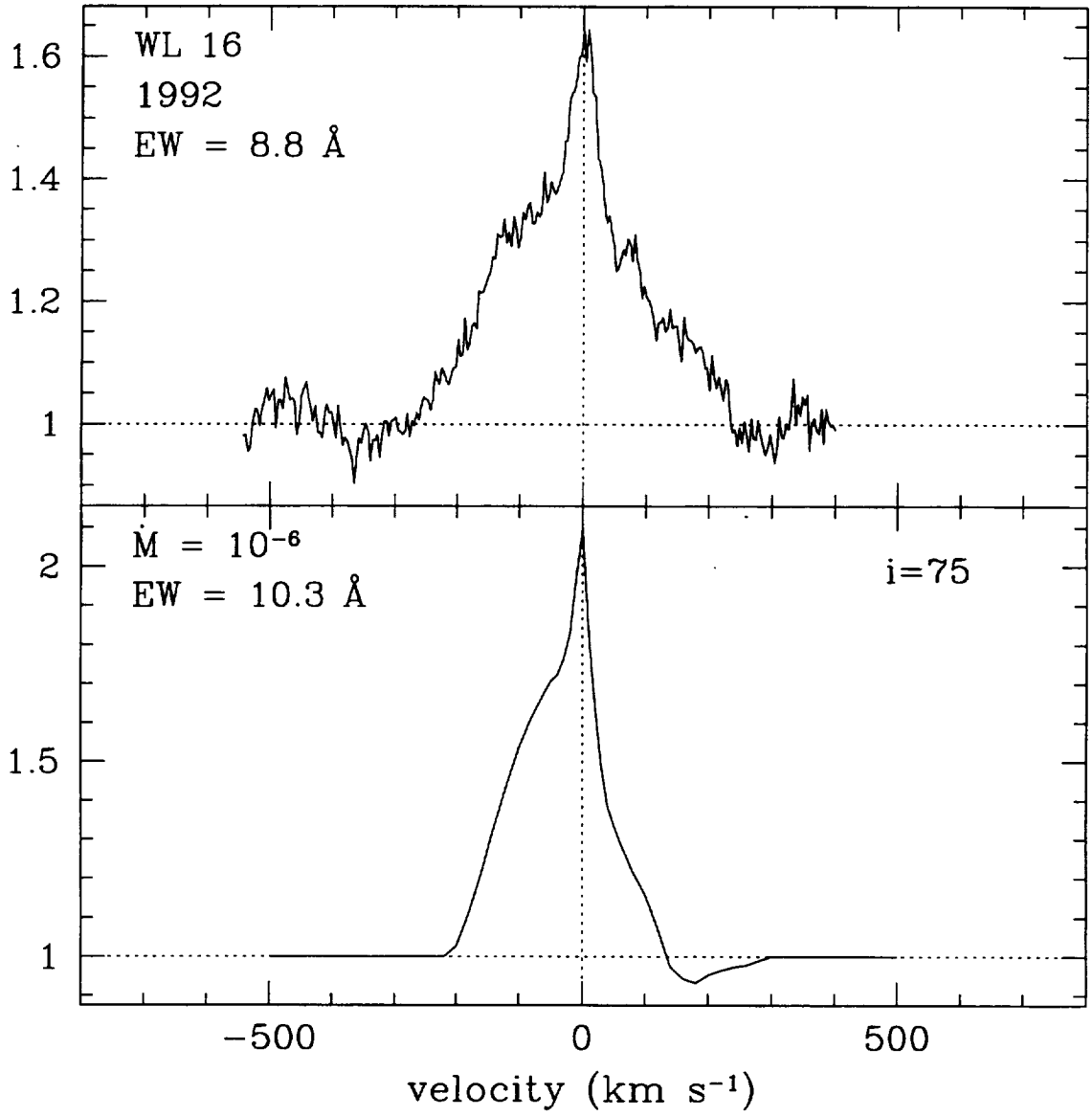

Figure 8: Comparison of model Brγ profile with observed profile for the embedded object WL 16 from Najita et al. (1996).

Publications supported by this grant

1993 The Embedded Young Stars in the Taurus-Auriga Molecular Cloud. I. Models for Spectral Energy Distributions, S.J. Kenyon, N. Calvet, & L. Hartmann, ApJ, 414, 676

1993 The Embedded Young Stars in the Taurus-Auriga Molecular Cloud. II. Models for Scattered Light, S.J. Kenyon, B.A. Whitney, M. Gomez, & L. Hartmann, ApJ, 414, 773

1994 Protostellar Collapse in a Self-Gravitating Sheet, L. Hartmann, A.P. Boss, N. Calvet, & B. Whitney 1994, ApJL, 430, L49

1994 Flat Spectrum T Tauri Stars: The Case for Infall, N. Calvet, L. Hartmann, S.J. Kenyon, & B.A. Whitney, ApJ, 434, 330

1995 The FU Orionis Outburst as a Thermal Accretion Event: Observational Constraints for Protostellar Disk Models, K.R. Bell, D.N.C. Lin, L.W. Hartmann, & S.J. Kenyon, ApJ, 444, 376

1996 Sheet Models of Protostellar Collapse, L. Hartmann, N. Calvet, & A.P. Boss, ApJ, 464, 387

1997 The Structure and Emission of Accretion Disks Irradiated by Infalling Envelopes, P. D'Alessio, N. Calvet, & L. Hartmann, ApJ, 474, 397

1997 Disk Accretion and the Stellar Birthline, L. Hartmann, P. Cassen, & S.J. Kenyon, ApJ, 475, 770

1997 Near-Infrared Emission of Protostars, N. Calvet, L. Hartmann, & S.E. Strom, ApJ, 481, 912

1997 Magnetospheric Accretion Models for the Hydrogen Emission Lines of T Tauri Stars, J. Muzerolle, N. Calvet, & L. Hartmann, ApJ, in press

References

Adams, F.C., Lada, C.J., & Shu, F.H. 1987, ApJ, 312, 788

Andre, P., Ward-Thompson, D., & Barsony, M. 1993, APJ, 406 122

Beckwith, S.V.W., & Birk, C.C. 1995, ApJ, 449, L59

Calvet, N., Hartmann, L., Kenyon, S., & Whitney, B. 1994, ApJ, 434, 330

Calvet, N., Hartmann, L., & Strom, S. 1997, ApJ, 481, 912

Casali, M.M., & Eiroa, C. 1996, A&A, 306, 427

Cassen, P., & Moosman, A. 1981, Icarus, 48, 353

Chick, K.M., Pollack, J.B., & Cassen, P. 1995, ApJ, submitted

D'Alessio, P., Calvet, N., & Hartmann, L. 1997, ApJ, in press

Gahm, G.F., Loden, K., Gullbring, E., and Hartstein, S. 1995, AA, 301, 89

Gledhill, T.M., & Scarrott, S.M. 1989, MNRAS, 236, 139

Grasdalen, G.L., Sloan, G., Stout, M., Strom, S.E., & Welty, A.D. 1989, ApJL, 339, L37

Hartmann, L., Boss, A.P., Calvet, N., & Whitney, B. 1994, ApJL, 430, L49

Hartmann, L., Calvet, N., & Boss, A.P. 1996, ApJ, 464, 387

Hartmann, L., Cassen, P., & Kenyon, S. 1997, ApJ, 475, 770

Hayashi, M., Ohashi, N., & Miyama, S. 1993, ApJ, 418, L71

Kenyon, S.J., Calvet, N., & Hartmann, L. 1993a, ApJ, 414, 676

Kenyon, S.J., & Hartmann, L. 1995, ApJS, 101, 117

Kenyon, S.J., Whitney, B., Gomez, M., & Hartmann, L. 1993b, ApJ, 414, 773

Lay, O.P., Carlstrom, J.E., Hills, R.E., & Phillips, T.G. 1994, ApJ, 434, L75

Muzerolle, J., Calvet, N., & Hartmann, L. 1997, ApJ, in press

Myers, P.C., Fuller, G.A., Goodman, A.A., & Benson, P.J. 1991, ApJ, 376, 561

Nakamura, F., Hanawa, T., & Nakano, T. 1995, ApJ, 444, 770

Palla, F., & Stahler, S.W. 1992, ApJ, 392, 667

Sargent, A.I., & Beckwith, S. 1991, ApJ, 382, L31

Shu, F.H. 1977, ApJ, 214, 488

Stahler, S.W. 1988, ApJ, 332, 804

Stapelfeldt, K.R., Burrows, C.J., Krist, J.E., Trauger, J.T., Hester, J.J., Holtzman, J.A., Ballester, G.E., Casertano, S., Clarke, J.T., Cristp, D., Evans, R.W., Gallagher, J.S. III, Griffiths, R.E., Hoessel, J.G., Mould, J.R., Scowen, P.A., Watson, A.M., & Westphal, J.A. 1995, ApJ, L Aug 20.

Weintraub, D.A., Kastner, J.H., & Whitney, B.A. 1995, preprint

Whitney, B. A., & Hartmann, L. 1993, ApJ, 402, 605